ACS Catalysis

Research Article

pubs.acs.org/acscatalysis

Highly Active and Stable Pt_3Rh Nanoclusters as Supportless Electrocatalyst for Methanol Oxidation in Direct Methanol Fuel Cells

Bhuvanendran Narayanamoorthy,[†] Kasibhatta Kumara Ramanatha Datta,[§] Muthusamy Eswaramoorthy,[‡] and Subramanian Balaji*,[†]

[†]Department of Chemistry, Faculty of Science, Sri Chandrasekharendra Saraswathi Viswa Mahavidyalaya (SCSVMV University), Enathur, Kanchipuram 631 561, India

[‡]Nanomaterials and Catalysis Lab, Chemistry and Physics of Materials Unit, Jawaharlal Nehru Centre for Advanced Scientific Research (JNCASR), Bangalore 560 064, India

[§]Regional Centre of Advanced Technologies and Materials, Faculty of Science, Department of Physical Chemistry, Palacky University, 771 46 Olomouc, Czech Republic

Supporting Information

ABSTRACT: The supportless PtRh nanoclusters (Pt_3Rh NC) were prepared using formic acid reductant. High-resolution transmission electron microscopy (HRTEM) showed individual particle sizes less than 7 nm, and energy-dispersive X-ray (EDX) analysis confirmed a 3:1 ratio of Pt and Rh. The as-prepared Pt_3Rh NC exhibited an improved activity and durability toward electrocatalytic oxidation of methanol (MOR) and possesses greater CO tolerance than conventional PtRu and other Pt-based MOR catalysts. For comparison, the Vulcan carbon supported (Pt_3Rh NC/VC) catalyst was prepared under identical conditions and used for MOR. The supportless Pt_3Rh NC catalyst possessed mass activity of 1392.5 mA mg^{-1} with an I_f/I_b ratio of 2.61, which is nearly 3-fold higher than the Pt_3Rh NC/VC and also comparable to the benchmark MOR catalysts. The surface poisoning rate was found to be relatively smaller compared to the standard PtRu/C catalysts (δ = 0.0044% s^{-1}). The activation energy for MOR was found to be 22.5 kJ mol^{-1}. The durability study for 4000 potential cycles in an acidic solution showed that nearly 78% of mass activity has been retained. The supportless Pt_3Rh NC has much improved activity and stability compared to both Pt_3Rh NC/VC and standard PtRu MOR catalysts. Therefore, the supportless Pt_3Rh NC could be seen as a potential electrocatalyst for methanol oxidation due to high activity, enhanced stability, and diminished poisoning of the Pt surface, which is stabilized in the presence of Rh in nanocluster morphology.

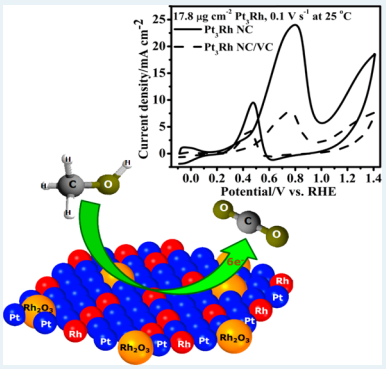

KEYWORDS: *PtRh nanoclusters, methanol oxidation, mass activity, activation energy, durability*

INTRODUCTION

Methanol is one of the sustainable bioenergy sources and has a high energy density (3800 kcal/l) compared to hydrogen (658 kcal/l at 360 atm), and therefore, direct methanol fuel cells are gaining more attention for automobile and portable applications.[1,2] In direct methanol fuel cells (DMFC), methanol is oxidized at the anodic compartment, whereas oxygen from air is reduced at the cathode. Methanol oxidation is a catalyst-driven process, and the products formed are HCHO, HCOOH, and CO_2 along with some intermediates.[3−5] Platinum is the most widely tested catalyst for methanol oxidation, but the Pt surface is immediately poisoned by adsorbed CO, an intermediate prior to CO_2 formation during oxidation.[6] In order to overcome the sluggish kinetics and catalyst surface poisoning of precious catalyst materials such as Pt, alloying with other nonprecious metals are being investigated with an aim to enhance both the mass activity and CO tolerance. The addition of second element to Pt can alter the electronic properties and interatomic bond distance and hence influence the overall catalytic properties of pure Pt.[7−9]

A commonly used strategy to design a highly efficient catalyst for DMFCs is using bi/multimetallic nanoparticle system. Bimetallic nanoparticle alloys are more attractive due to high catalytic activity and selectivity compared to the individual components, and because the property of bimetallic alloy can be tuned by varying their composition, the activity enhancement is still possible within a given pair of metals.[10−12] The synergistic effect of bimetallic nanocatalysts was discussed by many researchers. Since the transition metals with half-filled d-bands (viz., Ru, Pd, Rh) reveal high activity, the CO-poisoned Pt can be regenerated via the reaction of surface CO with oxygen-containing species such as Ru to convert CO to CO_2.[13−16] PtRu bimetallic catalysts have been widely

Received: May 8, 2014
Revised: August 27, 2014
Published: September 2, 2014

   dx.doi.org/10.1021/cs500628m | ACS Catal. 2014, 4, 3621−3629

investigated for their good catalytic activity toward methanol oxidation. However, in the presence of methanol, Ru leaches out from PtRu, reducing the activity of the electrocatalyst in the anodic part, and Ru crossover toward the cathode side inhibits the kinetics of oxygen reduction, hence reducing the overall cell performance.[17] In single-cell DMFC experiments, the polarization curves recorded with pure Pt and Ru-contaminated Pt cathodes have shown an unrecoverable performance loss due to Ru crossover.[18] Metals such as Rh, Ni, Sn, and Mo have also been reported for enhanced catalytic activity toward methanol oxidation.[19−21]

The PtRh bimetallic nanoparticle system has been reported by many researchers because of its enhanced catalytic activity toward oxidation reactions involving C−C bond breaking. It was found that the CO poisoning effect over Pt can be inhibited using rhodium oxide, by weakening the adsorption of CO on neighboring Pt atoms and promote the oxidation of CO to CO_2. Bulk PtRh alloy found to exhibit an excellent catalytic activity for small alcohol oxidations than pure Pt.[22−24] Many researchers have observed that the presence of Rh nanoparticles along with Pt in the form of binary, ternary, and quaternary electrocatalysts influence the catalytic activity toward oxidation of methanol and ethanol for fuel cell applications due to C−C and C−H bond-breaking ability of Rh.[25−31] Zhang et al. have reported the synthesis of three-dimensional PtRh alloy porous nanostructures with 2−3 nm sized nanoparticles in the presence of oleyalamine by hydrothermal synthesis at 240 °C and studied the MOR. They found better catalytic activity for the composition of ∼16 at% of Rh, yet the ratio of forward current to backward current (I_f/I_b) gets reduced to ∼30% of its initial value (5.31 to 1.44) after 100 potential cycles, indicating the poor CO tolerance of PtRh porous catalyst.[32] Choi et al. have reported that PtRh and PtRuRh nanoparticles of size 3−4 nm prepared by borohydride reduction and found that PtRuRh possesses a higher power density of 197 mW cm^{-2} than PtRu electrocatalyst (169 mW cm^{-2}) in single-cell DMFC.[33] Park et al. have studied the catalytic activity of PtRh and PtRuRhNi alloy of ∼4.5 nm sized nanoparticles using single cell system for MOR, and they have concluded that presence of Rh may influence the regeneration of active Pt surface.[34,35]

However, the reduced activity and poor stability issues of bimetallic catalyst systems still need to be dealt with. To surmount this problem, before designing new alloy catalysts, theoretical calculations could be used to predict the promising candidates for further study. Baraldi et al. have theoretically predicted that PtRh (111) bimetallic nanoclusters could enhance the chemical reactivity of the catalyst in fuel cell reactions.[36] The electronic structure and stability of PtRh nanoparticles were analyzed by first-principle calculations by Yuge et al., and they observed that PtRh nanoparticles are energetically preferred compared to PtRh bulk alloys.[37] These theoretical investigations have predicted that nanoclusters of PtRh may provide an enhanced stability where Rh acts as a stabilizer for Pt clusters. Therefore, PtRh nanoclusters might prove to be an active and stable electrocatalyst for methanol oxidation in DMFCs, and tuning the atomic composition between Pt and Rh may also play a key role in determining the performance of the catalyst.

In this work, we have prepared the Pt_3Rh nanocluster by a slow reduction approach and surface characterized using X-ray diffraction analysis (XRD), X-ray photoelectron spectroscopy (XPS), field emission-scanning electron microscopy (FE-SEM), high resolution-transmission electron microscopy (HR-TEM), and energy-dispersive X-ray analysis (EDX). Because capping agents and stabilizers may adhere to the surface and may poison the electrocatalyst, Pt_3Rh nanoclusters were prepared by adopting an environmentally benign approach in the absence of any capping agents using formic acid as the mild reducing agent. Furthermore, the ratio of Pt/Rh chosen in this study is optimized from different atomic weight percentage compositions of Pt and Rh on the basis of its electrochemical activity. The prepared Pt_3Rh NC was used as the supportless catalyst for methanol oxidation in sulfuric acid medium. The electrochemical activity and stability of the prepared nanoclusters was studied using cyclic voltammetry and chronoamperometry techniques at different temperatures, and the obtained results are compared with an in-house prepared Vulcan carbon supported Pt_3Rh NC catalyst (Pt_3Rh NC/VC) under identical conditions. The kinetic and durability parameters were determined and compared with standard benchmark MOR catalysts so far reported (Table S1, Supporting Information).[38−42]

EXPERIMENTAL METHODS

Hexachloro platinum(IV) acid hexahydrate (H_2PtCl_6. $6H_2O$), rhodium(III) chloride ($RhCl_3$), and formic acid (98%) were purchased from Sigma-Aldrich. Vulcan carbon-XC-72 was used as carbon support and received as complementary pack from Cabot (I) Ltd. Nafion perfluorinated polymer resin solution (5 wt %, Sigma-Aldrich), sulfuric acid (Rankem), methanol (98%, Merck), and absolute ethanol (Merck) were used as received. All solutions were prepared using Millipore (18 MΩ cm) distilled water. All the materials were used as received.

Pt_3Rh nanoclusters were synthesized as follows: An aqueous solution of $H_2PtCl_6.6H_2O$ (24 mg) and $RhCl_3.H_2O$ (6 mg) was taken (20 mL) in a beaker, 1 mL of formic acid (1.2 M) was added, and the resulting mixture was kept aside for 72 h at room temperature. In this synthesis procedure, the color change of Pt_3Rh mixture was observed from red orange to brown orange after 1 h and then completely turned to black brown precipitate. The particles were separated by centrifugation followed by washing with a mixture of water and methanol repeatedly three times. Finally, the product was collected and dried in an air oven at 60 °C for 2 h. Here, the percentage of metal composition between Pt and Rh was maintained based on the atomic weight of each element. For the preparation of Vulcan carbon supported catalysts, 7.5 mg of Vulcan carbon XC-72 (VC) was added at the initial stage of above synthesis procedure.

Powder X-ray diffraction (XRD) patterns were recorded using Bruker-D8 diffractometer using Cu Kα radiation, (λ = 1.54 Å, step size: 0.02 for supportless Pt_3Rh NC and 0.005 for Pt_3Rh NC/VC; current: 30 mA; and voltage: 40 kV), and the mean nanoparticle size was calculated by applying the Debye−Scherrer equation. Field-emission scanning electron microscopy (FE-SEM) images and energy-dispersive X-ray patterns (EDX) were obtained by means of FEI (Nova-Nano SEM-600, Netherlands). For transmission electron microscope (TEM) analysis, the sample was redispersed in absolute ethanol by sonication before drop casting on a carbon-coated copper grid. TEM and high-resolution TEM (HR-TEM) measurements were carried out using FEI Tecnai 30G2 (300 kV) high resolution transmission electron microscope. X-ray photoelectron spectroscopic (XPS) measurements were performed using X-ray photoemission spectrometer (Omicron Nano-

dx.doi.org/10.1021/cs500628m | ACS Catal. 2014, 4, 3621−3629

technology, Germany) using Al Kα (1486.7 eV) as X-ray source operating at 100 W.

A double jacketed three electrode electrochemical cell consisting of rotating disc glassy carbon (RDE-GC, 5 mm diameter from Pine) as the working electrode, double junction Ag/AgCl (Pine, 10% KNO_3) as the reference electrode, and 0.2 mm platinum sheet (1 cm^2) as the counter electrode was used to investigate the electrocatalytic activity of the catalyst. As a standard practice and for convenience, all electrode potentials are reported versus RHE. The voltammetry experiments were conducted with a computer interfaced electrochemical workstation (Potentiostat/Galvanostat, Autolab PGSTAT-128N) in conjunction with a rotator (Pine). The cell temperature was controlled by circulating water in the outer jacket using cryostat/thermostat equipment (Equibath, India).

The catalyst ink was prepared by dispersing 0.5 mg of the catalyst in 1 mL of absolute ethanol and ultrasonicating for 3 min to get a homogeneous dispersion. Then, 7 μL of the catalyst ink was pipetted out on to a mirror finished surface of RDE-GC (metal loading of about 17.8 μg cm^{-2}) and covered with a 5 μL coating of 0.05 wt % Nafion solution. Prior to coating, the GC surface was polished with 0.05 μm alumina slurry washed with ethanol and water and then subjected to ultrasonic agitation for 5 min in deionized water. The cyclic voltammograms were recorded in N_2 saturated 0.5 M H_2SO_4 at the scan rate of 0.1 V/s between −0.1 to 1.2 V at 25 °C. The electrochemical surface areas (ECSA) were calculated by measuring the charge associated with the H_{ads} (Q_H) between −0.08 and 0.2 V and assuming Q_{ref} =210 μC cm^{-2}, which is generally accepted for polycrystalline Pt electrodes. The ECSA of Pt_3Rh was calculated based on the following equation[43]

$$\mathrm{ECSA} = \frac{Q_H}{(Q_{ref} \times m)}$$

where Q_H is the charge for H-desorption (μC cm^{-2}), m is the mass of Pt_3Rh loading (17.8 μg cm^{-2}) over GC electrode, and Q_{ref} is the charge required for the monolayer adsorption of hydrogen on a Pt surface (210 μC cm^{-2}).

Methanol oxidation reaction (MOR) was investigated by CV studies in N_2 saturated 0.5 M H_2SO_4 + 0.5 M methanol at a sweep rate of 100 mV/s between 0.0 to 1.0 V at 25 °C. The thermodynamic parameters were calculated by recording CVs at different temperatures (25, 35, 45, 55, and 65 °C). The stability and poisoning rate of the catalysts for methanol oxidation were estimated by chronoamperometry at a potential of 0.8 V at 25 °C. The long-term stability of catalysts was checked by continuous potential cycling between 0.2−1.0 V at the scan rate of 0.1 V s^{-1} in N_2-purged 0.5 M H_2SO_4 + 0.5 M methanol at 25 °C for both supportless and VC supported Pt_3Rh.

RESULTS AND DISCUSSION

The morphology and composition of the catalysts are determined by field emission scanning electron microscopy (FESEM), transmission electron microscopy (TEM), energy-dispersive X-ray (EDX), and X-ray photoelectron spectroscopy (XPS) analyses. EDX spectrum of catalyst (Figure S1, Supporting Information) indicates that Pt and Rh are the major elements along with small amounts of carbon and oxygen, respectively. The atomic weight percentages of Pt and Rh in the sample were found to be 76 and 23%, respectively, corresponding to a 3:1 atomic ratio of Pt:Rh in the catalyst. X-ray diffraction pattern of the supportless Pt_3Rh catalyst exhibits (111), (200), (220), and (311) reflections that are consistent with the metallic platinum having face-centered-cubic (fcc) structure (Figure 1).[44] The catalyst dispersed over VC support

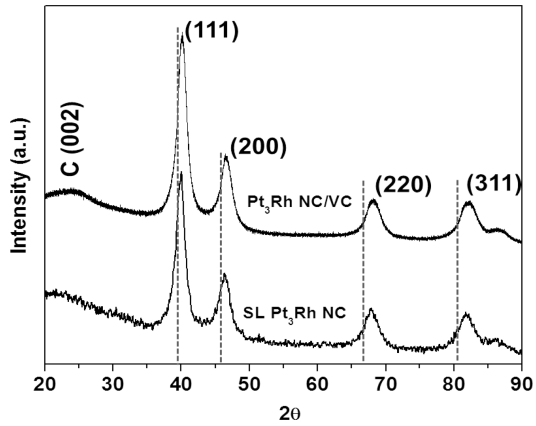

Figure 1. XRD patterns of supportless and VC-supported Pt_3Rh nanoclusters.

also displayed similar peak positions (40.4° for (111) plane) to that of supportless nanocluster, in addition to the peak at 23.8° corresponding to (002) plane of hexagonal carbon structure. We observed that the peak due to (111) at 39.8 ° is slightly shifted to a higher angle by ∼0.6 ° (40.4 °) for both the catalysts.[35] Similarly the same trend was also observed in 2θ values of the (200), (220), and (311) peaks. The higher angle shift of the peaks with decreased d-spacing value and contraction of lattice constant indicates the incorporation of Rh atoms into the Pt fcc structure, accounting the alloy formation between Pt and Rh.[35] Further, we can observe that the intensity of (111) plane is much stronger than the (200) plane, which is normally expected for a three-dimensional randomly oriented assembly.[45] This is further supported from FESEM (Figure S2, Supporting Information) and TEM images (Figure 2). The nanoparticle size estimated from Scherrer equation for the (111) peak position is about 4 nm, which is consistent with that measured value from the respective TEM images (Figure 2a).

FESEM images (Figure S2a,b, Supporting Information) of the SL Pt_3Rh showed spherical assemblies of the catalyst, which is further made up of smaller nanoparticles typically exhibiting the cluster morphology. The Pt_3Rh/VC shows a uniform distribution of Pt_3Rh nanoparticles embedded over the surface of carbon support (Figure S2c,d, Supporting Information). For SL Pt_3Rh, the homogeneous distribution of Pt and Rh throughout the structure is clearly seen from the elemental mapping (Figure S3, Supporting Information). The TEM image of the supportless Pt_3Rh (Figure 2a) shows particles of the sizes less than 7 nm that are assembled to form a network. The inset of histogram in TEM image (Figure 2a) shows the average particle size was found to be around 3.4 nm with the standard deviation of ±0.74 nm. The HRTEM shows the lattice fringe spacing of 0.22 nm (Figure 2b), which corresponds with the d-spacing obtained from XRD corresponding to the (111) plane of the SL Pt_3Rh sample.

The XPS analysis was performed to understand the nature and composition of the catalyst. The obtained binding energies at 70.9 and 74 eV correspond to $4f_{7/2}$ and $4f_{5/2}$ regions of Pt (Figure S4a, Supporting Information). Also, the Pt (4d) region

dx.doi.org/10.1021/cs500628m | ACS Catal. 2014, 4, 3621−3629

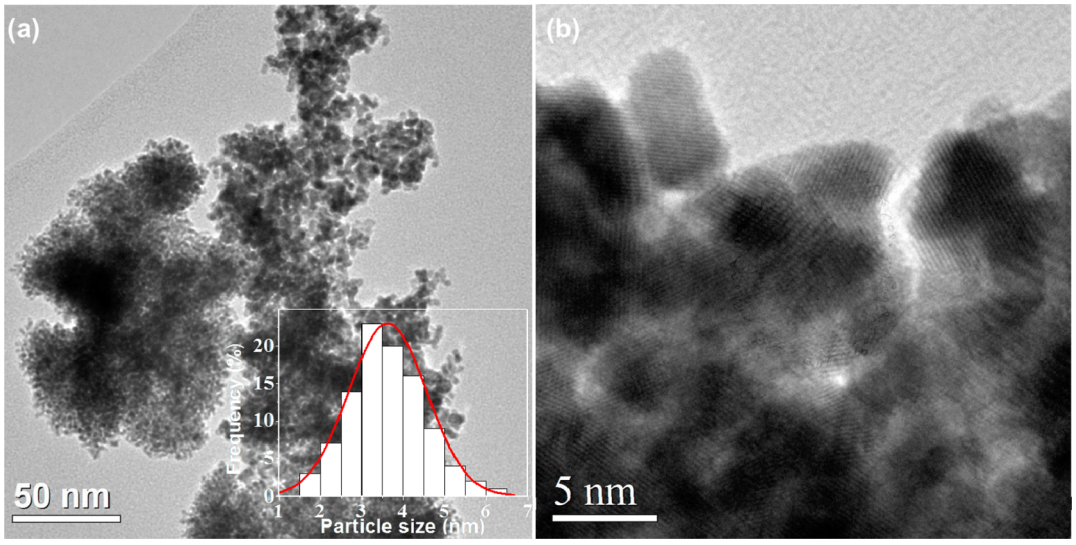

Figure 2. (a) TEM with histogram and (b) HRTEM images of supportless Pt_3Rh nanoclusters.

is characterized by a doublet which arises from spin−orbit coupling. The binding energies at 314.2 and 331 eV correspond to Pt $4d_{5/2}$ and $4d_{3/2}$ states, respectively. The presence of $4f_{7/2}$ and $4d_{5/2}$ in the XPS spectra shows that Pt is in metallic state.[46] In addition, rhodium peaks appear at 307.1 and 312 eV, respectively, corresponding to Rh (3d) region (Figure S4b, Supporting Information). We observed the overlapping of Rh $3d_{3/2}$ peak by Pt $4d_{5/2}$. This could be due to the presence of rhodium oxide species in the sample as observed by Saidani et al.[47] XPS results indicate a mixture of metallic and oxide state of Rh, and this mixture was shown to enhance the oxidation of carbon monoxide and could play a role as an oxygen source for CH_3OH oxidation as explained by Park et al.[35] Also the atomic weight percentage composition calculated from XPS analysis confirms a 3:1 ratio of Pt and Rh in the Pt_3Rh nanocluster.

The elemental composition between the supportless PtRh NC has been varied as 3:1, 1:1, and 1:3 in terms of atomic wt % and was optimized on the basis of the electrocatalytic activity in terms of ECSA. From the CVs (Figure S5, Supporting Information), the higher ECSA was found (114.4 $m^2\ g^{-1}$) for SL Pt_3Rh for the metal loading of 40.8 $\mu g\ cm^{-2}$. The values of ECSA were tabulated and compared for all the three catalysts and given as the inset of Figure S5, Supporting Information. This optimized composition was taken for further electrochemical investigations on methanol oxidation. Figure 3 shows the CVs of supportless and VC supported Pt_3Rh NC recorded in N_2-saturated 0.5 M H_2SO_4 between 0.0 and +1.2 V at 25 °C. In order to remove any surface contaminations from Nafion solution and to obtain a stable CV pattern, the catalyst coated RDE electrode was subjected to potential cycling for 10 times at the scan rate of 0.1 $V\ s^{-1}$.[48,49] The electrochemically active surface area (ECSA) of these catalysts were obtained from the respective CVs by integrating the hydrogen desorption region in the positive potential scan from −0.08 to 0.20 V, subtracting the double-layer charging current, and dividing the resulting columbic charge associated with the hydrogen monolayer desorption by 210 $\mu C\ cm^{-2}$, corresponding to the bulk polycrystalline Pt surface as given in equation (refer to the ECSA equation in Experimental Methods).[43] The oxide formation region observed during the oxidation sweep indicates both Pt−O and Rh−$O(OH)_3$ formed between 0.7 to 1.0 V for supportless Pt_3Rh NC and VC-supported Pt_3Rh NC. This

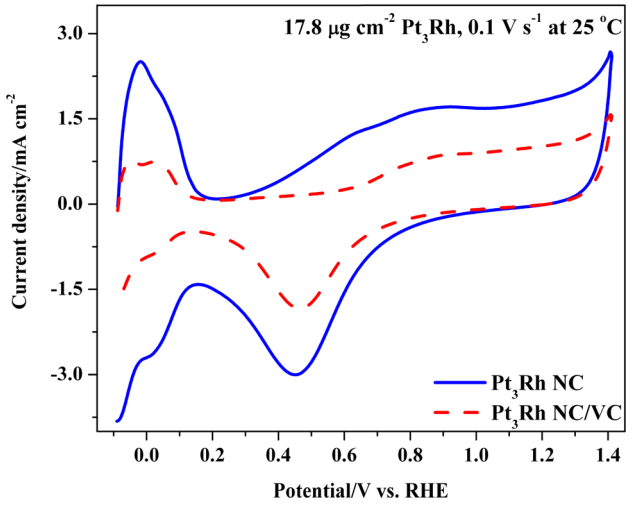

Figure 3. Cyclic voltammograms of supportless and VC-supported Pt_3Rh NC in N_2 saturated 0.5 M H_2SO_4 at 25 °C.

potential range for oxide formation is comparable to the reported value.[30] The obtained ECSA was found to be 154.4 and 63.1 $m^2\ g^{-1}$ for supportless and VC supported Pt_3Rh NC, respectively. The larger difference in ECSA could be due to the partially buried Pt_3Rh NC over carbon surface. Also, the values of ECSA are comparable with various Pt nanostructures and standard Pt/C catalysts.[50,51]

Figure 4 depicts the typical cyclic voltammograms of methanol oxidation obtained for supportless and VC-supported Pt_3Rh NC coated over GC-RDE in N_2 saturated 0.5 M H_2SO_4 + 0.5 M methanol scanned in the potential window of 0.0 and 1.0 V at the scan rate of 0.1 $V\ s^{-1}$ and at 25 °C. The methanol oxidation current density was obtained by dividing the peak current values by the geometrical surface area of the working electrode. The formation of first oxidation peak during the positive going scan is usually ascribed to the oxidation of methanol to smaller short chain organic molecules and carbon monoxide. The second oxidation peak formed during the negative going scan is ascribed to the reoxidation of the formed organics by the OH radicals adsorbed over the catalyst surface. The MOR forward peak current density and peak potential

dx.doi.org/10.1021/cs500628m | ACS Catal. 2014, 4, 3621−3629

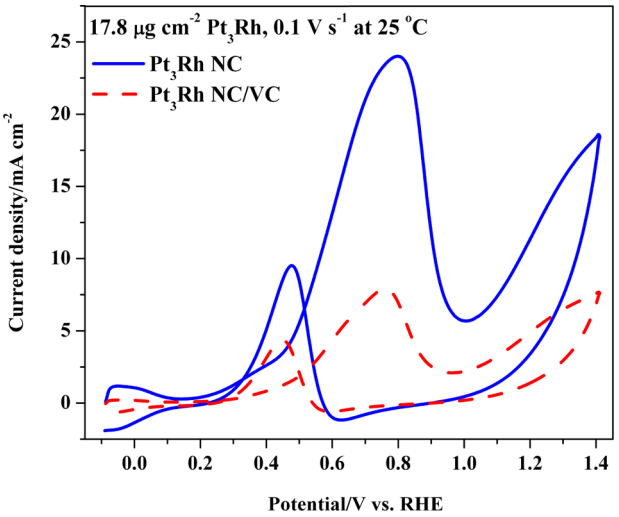

Figure 4. Cyclic voltammograms of supportless and VC supported Pt_3Rh NC in N_2 saturated 0.5 M H_2SO_4 + 0.5 M methanol at 25 °C.

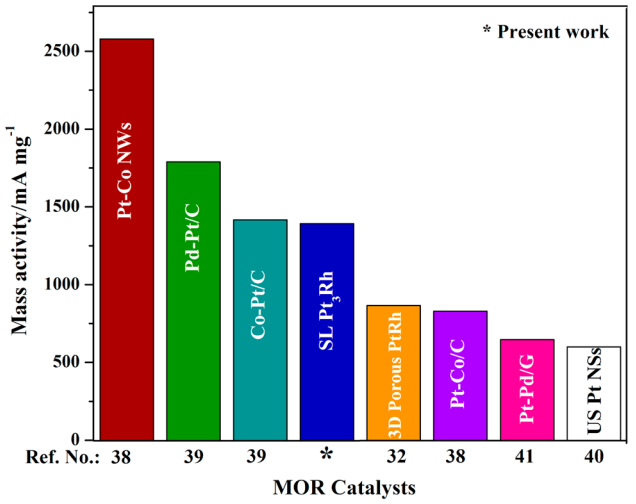

Figure 5. Comparison of mass activities of MOR for Pt-based catalysts from various literatures.

were found to be 24.86 mA cm^{-2} and 0.80 V, respectively, which is about 3.2 times higher in current density and 40 mV positively shifted than Pt_3Rh NC/VC (7.89 mA cm^{-2} and 0.76 V) and almost the same magnitude of forward peak potential reported for Pt_{50}-Ru_{50}/3D nanoporous graphitic carbon, but the forward peak current density of supportless Pt_3Rh NC is nearly three times higher than the Pt−Ru system (8.93 mA cm^{-2}).[52] It is to be noted that Pt−Ru is the standard and the best-performing benchmark electrocatalyst for methanol oxidation, and Pt_3Rh is now found to be better than Pt−Ru in terms of current density. Furthermore, the onset potential of the forward oxidation peak for supportless Pt_3Rh NC is quite earlier by 20 mV compared to VC supported Pt_3Rh NC catalyst, indicating more favorable methanol oxidation on the supportless catalyst surface. Here, the lower onset potential implies that breaking of C−H bonds and the subsequent removal of intermediates such as CO_{ad} which undergoes oxidation with OH_{ad} supplied by the Rh active site[30] and hence the oxidation of methanol becomes more favorable over the supportless Pt_3Rh NC catalyst surface.

The ratio of the forward oxidation peak current density (j_f) to the reverse oxidation peak current density (j_b) can be used to describe the CO tolerance of the catalyst[38] i.e. from the CVs of MOR, the j_f/j_b ratio was found to be 2.86 for supportless Pt_3Rh NC and 1.88 for Pt_3Rh NC/VC. The higher value of j_f/j_b ratio for supportless Pt_3Rh indicates an effective methanol oxidation and lesser poisoning of the catalyst surface compared to the Pt_3Rh NC/VC and standard Pt/C catalysts.[41] This indicates that Pt_3Rh NC has an improved activity toward MOR and in fact higher than the state of the art of Pt−Ru/C catalysts (0.87−0.96)[53,54] and the supportless Pt-based catalysts as seen from various reported values.[32,38−42]

The mass activities (MA) of the catalysts were calculated using the actual catalyst loading (17.8 μg cm^{-2}) from the forward peak current values. Figure 5 shows the comparison of mass activity of Pt_3Rh NC catalyst with other MOR benchmark catalysts having highest MA values insofar reported literature. Among these catalysts, supportless Pt_3Rh stands in fourth position in terms of MA, but it has appreciable j_f/j_b ratio of 2.41, which is nearly 2 times higher than the standard catalysts shown in Figure 5. Table S1 (Supporting Information) provides the comparison of MA and j_f/j_b ratio for supportless Pt_3Rh NC with VC supported Pt_3Rh NC catalysts and various Pt-based nanostructures from a recent literature survey. Hence, it can be concluded that Pt_3Rh NC has an enhanced catalytic activity toward methanol oxidation than both pure Pt and Pt−Ru catalysts.[43,55] This could be attributed due to the higher surface energy of Rh than Pt that can prevent the CO masking and weaken the OH adsorption on Pt in Pt_3Rh NC as shown by Baraldi et al. and Friebel et al. by DFT calculations.[36,56] Also, the electronic effects (shift in d-electron density of Pt due to alloying with Rh) might have contributed to the improved activity of both the Pt_3Rh NC catalysts as compared to pure Pt/C standard catalysts reported in literatures.[41]

The CVs for supportless Pt_3Rh NC and Pt_3Rh NC/VC in N_2 saturated 0.5 M H_2SO_4 + 0.5 M methanol at 0.1 V/s scan rate at different temperatures from 25 to 65 °C are shown in the Figures S6 and S7, Supporting Information. Upon increasing the temperature, the onset potential has improved by 30 mV (0.15 to 0.12 V) for supportless Pt_3Rh NC showing the temperature-dependent activity of the catalyst. The MOR current densities obtained from the forward oxidation peaks found to vary from 24.86 to 36.67 mA cm^{-2} for supportless Pt_3Rh NC and 7.89 to 31.11 mA cm^{-2} for VC-supported Pt_3Rh NC. Compared with VC supported catalyst, supportless Pt_3Rh NC shows the saturated current plateau at a higher temperature range. The forward oxidation peak current density reaches a saturation (plateau) region for supportless Pt_3Rh NC, indicating that the desorption of methanol oxidation products is kinetically hindered at higher temperatures due to the fast disappearance of OH free radicals at elevated temperatures and that accumulated surface organics are further oxidized, as seen from the increasing trend of reverse oxidation peak current densities. Whereas Pt_3Rh over VC surface the oxidation products are likely to adsorb over carbon support than on the catalyst surface and hence giving a sharp peak for forward oxidation at higher temperatures. But then the reoxidation current also increases during the negative potential scan due to the immediate vicinity of the oxidation products. Therefore, with increase in temperature a decrease in j_f/j_b ratio from 2.61 to 1.25 and 1.88 to 1.06, respectively, for supportless Pt_3Rh NC and Pt_3Rh NC/VC were observed. Despite the decreasing trend against temperature supportless NC maintains a higher magnitude of j_f/j_b ratio compared to VC supported and

dx.doi.org/10.1021/cs500628m | ACS Catal. 2014, 4, 3621−3629

standard Pt/C catalysts.[40,42] Figure 6 shows the Arrhenius plots of log j_f vs $1/T$ constructed using the anodic (oxidation)

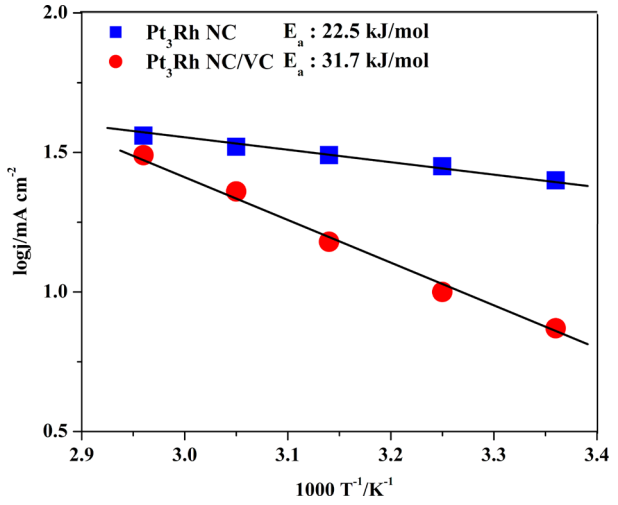

Figure 6. Arrhenius plots for MOR obtained at 25, 35, 45, 55, and 65 °C (current densities obtained from corresponding CV profiles for both supportless and VC-supported Pt_3Rh NC in O_2 saturated 0.5 M H_2SO_4 + 0.5 M methanol at a scan rate of 0.01 V s^{-1}).

current density obtained from corresponding CVs (Figures S5 and S6, Supporting Information) of both supportless and VC supported Pt_3Rh NC. The calculated activation energies for supportless Pt_3Rh NC and Pt_3Rh NC/VC were found to be 22.5 and 31.7 kJ mol^{-1}, respectively, which are comparable to the reported range of 20−95 kJ mol^{-1} for standard Pt and Pt−Ru catalysts.[57,58] The lower magnitude of activation energy for Pt_3Rh NC shows a more favored oxidation of methanol in acid medium.

The CO tolerance and poisoning rate of the Pt_3Rh NC during methanol oxidation were determined by chronoamperometry (CA) in N_2-saturated 0.5 M H_2SO_4 + 0.5 M methanol at a constant potential of 0.8 V for 2000 s. The CA curves for supportless Pt_3Rh NC and Pt_3Rh NC/VC catalysts recorded at 25 °C are shown in the Figure S8, Supporting Information. Initially, the oxidation currents of both the catalysts were gradually decreasing, and after ∼500 s, they remained stable. The overall current decay for supportless Pt_3Rh NC and Pt_3Rh NC/VC were found to be 86% and 97% respectively after 2000 s. It can be observed that the oxidation current loss is comparatively lesser for Pt_3Rh NC than VC-supported Pt_3Rh NC and supportless Pt nanostructures and conventional PtRu/C catalysts.[43,44] Also, the linear decay of the oxidation current at any time greater than 500 s may be specified by the long-term poisoning rate, δ:[55]

$$\delta = \frac{100}{I_0} \times \left(\frac{dI}{dt}\right)_{t>500s} (\%s^{-1})$$

where $(dI/dt)\ t_{>500s}$ is the slope of the linear portion of the current decay, and I_0 is the current at the start of polarization back extrapolated from the linear current decay. The calculated "δ" values for supportless and VC-supported Pt_3Rh NC were found to be 0.0011% s^{-1} and 0.0035% s^{-1}, respectively, showing the lower poisoning rate of Pt_3Rh NC catalyst toward MOR than VC-supported and standard PtRu/C MOR catalysts (δ = 0.0044% s^{-1}).[55,59] From chronoamperometry studies, it was observed that the supportless Pt_3Rh NC suffers lesser poisoning rate than the state of the art Pt−Ru/C catalysts for MOR.

Methanol oxidation is a complex six-electron transfer reaction involving many intermediates such as HCHO, HCOOH, $HCOOCH_3$, and CO and widely investigated and reported by many researchers.[60,61] Methanol undergoes oxidation to CO_2 electrochemically in a parallel pathway, as shown below.[3]

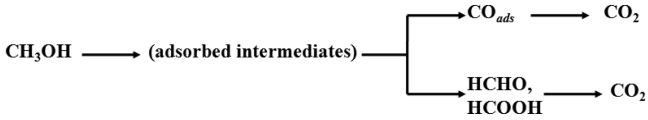

It is well-established that the initial adsorption of methanol over the Pt electrode surface begins at ∼0.2 V vs RHE for Pt electrode. At around 0.4 to 0.45 V vs RHE, Pt forms surface −OH groups with water molecules. After 0.45 V, the adsorbed organic intermediates, and CO is oxidized to CO_2. The rate of oxidation depends on the nature of the catalyst material, methanol concentration, temperature, electrode roughness, applied potential, and time of electrolysis.[62] When Pt-M bimetallic/alloy electrocatalysts are used, the "bifunctional mechanism" is found to be the reason for enhanced activity due to the formation of highly reactive surface hydroxyl groups on the active sites of the second metal (oxophilic metals such as Ru, Rh, etc.), which quickly oxidizes the adsorbed CO on Pt surface as shown below.[63]

(i) Dehydrogenation of methanol

$$Pt + CH_3OH(s) \rightarrow Pt\text{-}CH_3OH_{ads} \rightarrow Pt\text{-}CO_{ads} + 4H^+ + 4e^- \quad (1)$$

(ii) Dissociation of water

$$M + H_2O \rightarrow M\text{-}OH_{ads} + H^+ + e^- \quad (2)$$

(iii) Formation of CO_2

$$Pt\text{-}CO_{ads} + M\text{-}OH_{ads} \rightarrow Pt\text{-}M + CO_2 + H^+ + e^- \quad (3)$$

In this multistep bifunctional mechanism, the first step (eq 1) involves the adsorption of methanol on Pt active sites from bulk electrolyte solution and the successive dehydrogenation through the C−H bond breaking produces CO_{ads} as an intermediate. The second step (eq 2) involves dissociation of water molecules on active sites of secondary metal forming adsorbed $-OH_{ads}$ species. Finally, the adsorbed CO is oxidized by the −OH producing CO_2 (eq 3).

In electrochemical investigations, the calculation of Tafel slope provides the possible clue to understand the mechanistic pathway. The calculated Tafel slope values (Figure S9, Supporting Information) for supportless Pt_3Rh and Pt_3Rh/VC are respectively 126 and 153 mV/dec at low potential regions (0.2 to 0.5 V vs RHE). The Tafel slope value of supportless Pt_3Rh NC catalyst is near to the standard bimetallic Pt−Ru/C catalyst (115 mV/dec) employed for methanol oxidation.[64] This clearly shows that the mechanistic pathway goes predominantly through the formation of CO and oxidation of CO to CO_2 could be taken as the determining step.[3,64]

But, the Tafel slope value of Pt_3Rh/VC is higher by 27 mV/dec than supportless Pt_3Rh indicating a little higher hindrance at the electrode/electrolyte interface for electron transfer

dx.doi.org/10.1021/cs500628m | ACS Catal. 2014, 4, 3621−3629

reaction. When Vulcan carbon is used as the catalyst support for Pt_3Rh, the electrochemical surface area is reduced (when compared to supportless Pt_3Rh) due to the partially buried active sites in the Vulcan carbon matrix. Therefore, in VC-supported Pt_3Rh catalyst, the availability of carbon surface very near to the active sites of Pt_3Rh may affect the CO oxidation kinetics as follows: (i) The carbon substrate, which is known to adsorb CO strongly,[65] may keep the surface of PtRh constantly exposed to CO and is likely to hinder the oxidation kinetics of CO (a kind of film resistance at the electrode/electrolyte interface); (ii) Under the applied potential conditions, the carbon substrate itself undergoes electrochemical oxidation to form CO which increases the availability of CO in the immediate vicinity of the Pt_3Rh active sites;[66] (iii) Also, chronoamperometry results have shown that the CO poisoning rate of Pt_3Rh/VC (δ = 0.0035% s^{-1}) is nearly 3 times higher than the value of supportless Pt_3Rh (δ = 0.0011% s^{-1}). Hence, the oxidation of CO to CO_2 is proposed to be the rate-determining step on both supportless and VC-supported Pt_3Rh catalysts, and the observed difference in Tafel slope and activation energy values might be due to the spillover effect of adsorbed CO from the Vulcan carbon substrate and its resistance offered to the electrode/electrolyte interface.

The long-term accelerated durability test (ADT) of the supportless Pt_3Rh NC and Pt_3Rh NC/VC electrocatalysts was performed under continuous potential cycling between 0.2 and 0.8 V with a scan rate of 0.1 V s^{-1} at 25 °C. The CVs were recorded for every 1000 potential cycles for supportless Pt_3Rh NC (Figure 7) and Pt_3Rh NC/VC (Figure S10, Supporting Information) electrocatalysts up to 4000 cycles in N_2 saturated 0.5 M H_2SO_4 + 0.5 M methanol aqueous solution. The oxidation peak current densities after 4000 potential cycles for supportless and VC supported Pt_3Rh NC were found to be 18.99 and 1.58 mA cm^{-2}. It is clearly observed that there is no appreciable loss in methanol oxidation current density up to 2000 potential cycles for supportless Pt_3Rh (Figure 8), indicating that the presence of Rh in cluster morphology together with Rh_2O_3 help to regenerate the surface activity by way of CO oxidation (reduced potential energy barrier was said to be the reason for improved CO oxidation[67]) and after 4000 potential cycles it has retained around 77% of its initial limiting current (loss of 23%), which is comparatively 3.5 times higher than Pt_3Rh NC/VC and better than the reported Pt-based electrocatalysts (33% loss after 4000 PCs for supportless Pt−Pd tetrahedrons;[15] 40% loss after 300 PCs for Pt on Pd nanodendrites/graphene sheets;[41] 97% loss after 2000 PCs for PtRu/C).[68] The carbon substrate corrosion and masking of Pt surface by poisonous CO intermediate might have reduced the performance of VC supported Pt_3Rh.[69]

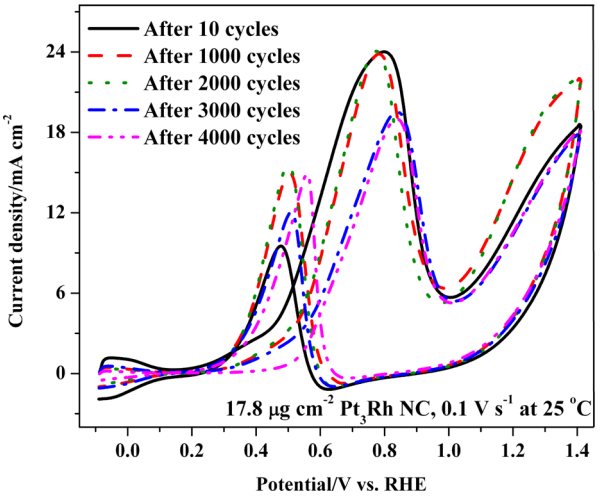

Figure 7. ADT—Cyclic voltammograms of supportless Pt_3Rh NC in N_2-saturated 0.5 M H_2SO_4 + 0.5 M methanol at 25 °C.

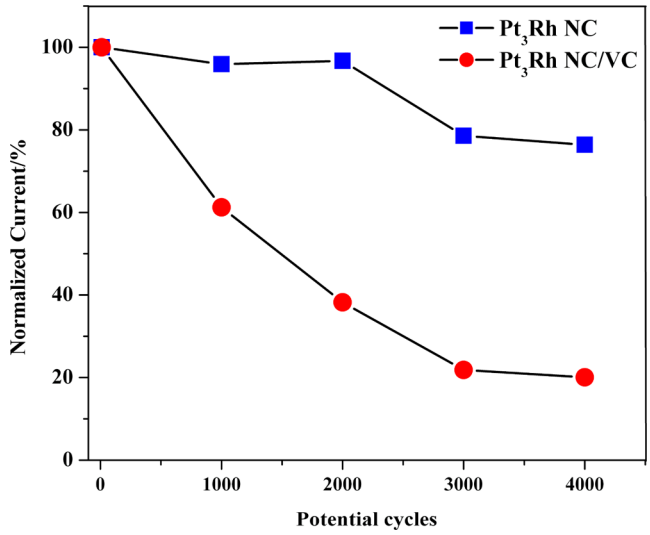

Figure 8. ADT—Normalized MOR current for supportless and VC-supported Pt_3Rh NC in N_2-saturated 0.5 M H_2SO_4 + 0.5 M methanol at 25 °C.

This higher loss in MA after the ADT for VC-supported Pt_3Rh might be due to carbon-corrosion-induced particle agglomeration or leaching out of Pt and Rh nanoparticles over the VC support. Also, it is observed that the ratio of j_f/j_b for both catalysts decreases slightly but not less than 1, indicating the better catalyzing ability of the electrocatalysts even after 4000 potential cycles. This activity retaining ability of Pt_3Rh NC could be due to the lower surface poisoning as seen from chronoamperometry. It is a noteworthy observation for supportless Pt_3Rh NC compared with so far reported standard Pt−Ru/C and Pt-based benchmark MOR electrocatalysts.[2,38−42,54] During potential cycling, there is no appreciable change in the onset potential and forward peak potential values for supportless Pt_3Rh NC and in fact ∼40 mV increase (positive shift) was observed in the onset potential for VC supported Pt_3Rh NC. The reason for the better durability of supportless Pt_3Rh NC for MOR could be due to the more durable nature of the Pt (111) facet[15,56] and also due to the surrounding Rh adatoms which favors the regeneration of active Pt surface by weakening Pt−O interactions as predicted by Friebel et al. through DFT calculations.[56] Therefore, it is concluded that supportless Pt_3Rh NC is one of the promising electrocatalysts for MOR in terms of activity and durability and in fact higher than, or comparable to, some of the best electrocatalyst systems for methanol oxidation.[32,40−43]

CONCLUSION

The Pt_3Rh nanoclusters were synthesized by a slow reduction process using formic acid as the reducing agent at room temperature for 72 h. From XRD, it was found that the Pt (111) plane is more predominant in both supportless and VC-supported Pt_3Rh NC. HR-TEM showed that the individual

dx.doi.org/10.1021/cs500628m | ACS Catal. 2014, 4, 3621−3629

nanoparticle size was less than 7 nm. The atomic weight percentage composition of Pt−Rh was confirmed by XPS and EDX analysis as 3:1. The catalytic activity of Pt_3Rh NC was examined toward MOR and compared with Vulcan carbon-supported Pt_3Rh NC and also with standard Pt-based nanostructures reported in the literature. Higher ECSA of 154.4 $m^2\ g^{-1}$ was obtained for supportless Pt_3Rh NC, and it is nearly 3 times higher than VC-supported Pt_3Rh NC. The observed MOR mass activity for supportless Pt_3Rh NC was found to be 1392.5 mA mg^{-1} with the j_f/j_b ratio of 2.61, which is higher than that of some of the benchmark catalysts hitherto reported. The durability of the electrocatalysts were studied by potential cycling, and nearly a 22% loss in mass activity was observed for supportless Pt_3Rh NC and 80% for VC-supported Pt_3Rh NC after 4000 cycles while the onset potential was nearly maintained. The high activity and stability could be attributed due to the presence of Rh adatoms in Pt (111) nanoclusters. It can be concluded that the supportless Pt_3Rh NC could effectively act as a potential electrocatalyst for methanol oxidation with high activity and enhanced durability in comparison to reported systems such as standard Pt/C and Pt−Ru MOR electrocatalysts.

■ ASSOCIATED CONTENT

Ⓢ Supporting Information

The Supporting Information contains a Table of mass activities of methanol oxidation for different electrocatalysts and EDX, FESEM, elemental mapping, XPS, CV at different temperatures, chronoamperometry plots, Tafel plots, and ADT-CVs. This material is available free of charge via the Internet at http://pubs.acs.org.

■ AUTHOR INFORMATION

Corresponding Author

*E-mail: prof.balaji13@gmail.com. Fax: +91-44-27264285. Tel.: +91-44-27264293.

Notes

The authors declare no competing financial interest.

■ ACKNOWLEDGMENTS

This work was financially supported by the Board of Research in Nuclear Sciences (BRNS), Department of Atomic Energy (DAE), Govt. of India, under Basic Sciences program through the sanction no. 2009/37/29/BRNS. S.B. profoundly thanks the management of SCSVMV University for having funded and created the necessary laboratory facilities to carry out this research project. B.N. thanks the CSIR, New Delhi for the award of a Senior Research Fellowship (SRF) through the sanction no. 09/1104(0001)/2013-EMR-I. In addition, K.K.R.D. acknowledges financial support by the Operational Program Research and Development for Innovations-European Regional Development Fund (project CZ.1.05/2.1.00/03.0058 of the Ministry of Education, Youth and Sports of the Czech Republic) and the Operational Program Education for Competitiveness-European Social Fund (project CZ.1.07/2.3.00/30.0004 of the Ministry of Education, Youth and Sports of the Czech Republic).

■ REFERENCES

(1) Gurau, B.; Smotkin, E. S. *J. Power Sources* **2002**, *112*, 339−352.
(2) Gonzalez, A. S.; Arco, E. B.; Escalante, J.; Sandoval, O. J.; Gamboa, S. A. *Int. J. Hydrogen Energy* **2012**, *37*, 1752−1759.
(3) Iwasita, T. *Electrochim. Acta* **2002**, *47*, 3663−3674.
(4) Iwasita, T. In *Handbook of Fuel Cells-Fundamentals, Technology and Applications* Vielstich, W., Gasteiger, H.A., Yokokawa, H., Eds.; John Wiley & Sons: New York, 2003; pp 610−612.
(5) Guo, J. W.; Zhao, T. S.; Prabhuram, J.; Chen, R.; Wong, C. W. *Electrochim. Acta* **2005**, *51*, 754−763.
(6) Luna, A. M. C.; Bonesi, A.; Triaca, W. E.; Baglio, V.; Antonucci, V.; Arico, A. S. *J. Solid State Electrochem.* **2008**, *12*, 643−649.
(7) Xia, B. Y.; Wu, H. B.; Wang, X.; Lou, X. W. *J. Am. Chem. Soc.* **2012**, *134*, 13934−13937.
(8) Ksar, F.; Ramos, L.; Keita, B.; Nadjo, L.; Beaunier, P.; Remit, H. *Chem. Mater.* **2009**, *21*, 3677−3683.
(9) Liu, H.; Tian, N.; Brandon, M. P.; Zhou, Z. Y.; Lin, J. L.; Hardacre, C.; Lin, W. F.; Sun, S. G. *ACS Catal.* **2012**, *2*, 708−715.
(10) Xu, Y.; Yuan, Y.; Ma, A.; Wu, X.; Liu, Y.; Zhang, B. *ChemPhysChem* **2012**, *13*, 2601−2609.
(11) Xu, J. B.; Zhao, T. S.; Yang, W. W.; Shen, S. Y. *Int. J. Hydrogen Energy* **2010**, *35*, 8699−8706.
(12) Suntivich, J.; Xu, Z.; Carlton, C. E.; Kim, J.; Han, B.; Lee, S. W.; Bonnet, N.; Marzari, N.; Allard, L. F.; Gasteiger, H. A.; Schifferli, K. H.; Horn, Y. S. *J. Am. Chem. Soc.* **2013**, *135*, 7985−7991.
(13) Palenzuela, A. V.; Centellas, F.; Garrido, J. A.; Arias, C.; Rodriguez, R. M.; Brillas, E.; Cabot, P. L. *J. Phys. Chem. C* **2010**, *114*, 4399−4407.
(14) Singh, B.; Murad, L.; Laffir, F.; Dickinson, C.; Dempsey, E. *Nanoscale* **2011**, *3*, 3334−3349.
(15) Yin, A. X.; Min, X. Q.; Zhang, Y. W.; Yan, C. H. *J. Am. Chem. Soc.* **2011**, *133*, 3816−3819.
(16) Huajie, H.; Dongping, S.; Xin, W. *Chin. Sci. Bull.* **2012**, *57*, 3071−3079.
(17) Gancs, L.; Hult, B. N.; Hakim, N.; Mukerjee, S. *Electrochem. Solid-State Lett.* **2007**, *10*, B150−B154.
(18) Chen, W.; Sun, G.; Guo, J.; Zhao, X.; Yan, S.; Tian, J.; Tang, S.; Zhou, Z.; Xin, Q. *Electrochim. Acta* **2006**, *51*, 2391−2399.
(19) Barranco, J.; Pierna, A. R. *J. Non-Cryst. Solids* **2008**, *354*, 5153−5155.
(20) Nishanth, K. G.; Sridhar, P.; Pitchumani, S.; Shukla, A. K. *Bull. Mater. Sci.* **2013**, *36*, 353−359.
(21) Wu, Y.; Wang, D.; Niu, Z.; Chen, P.; Zhou, G.; Li, Y. *Angew. Chem., Int. Ed.* **2012**, *51*, 1−6.
(22) Koch, D. F. A.; Rand, D. A. J.; Woods, R. *J. Electroanal. Chem.* **1976**, *70*, 73−86.
(23) Ross, P. N.; Kinoshita, K.; Scarpellino, A. J.; Stonehart, P. *J. Electroanal. Chem. Interface Electrochem.* **1975**, *59*, 177−189.
(24) De Tacconi, N. R.; Leger, J. M.; Beden, B.; Lamy, C. *J. Electroanal. Chem.* **1982**, *134*, 117−130.
(25) Lima, F. H. B.; Profeti, D.; Chatenet, M.; Riello, D.; Ticianelli, E. A.; Gonzalez, E. R. *Electrocatal.* **2010**, *1*, 72−82.
(26) Kawaguchi, T.; Rachi, Y.; Sugimoto, W.; Murakami, Y.; Takasu, Y. *J. Appl. Electrochem.* **2006**, *36*, 1117−1125.
(27) Du, W.; Wang, Q.; Lascala, C. A.; Zhang, L.; Su, D.; Frenkel, A. I.; Mathur, V. K.; Teng, X. J. *Mater. Chem.* **2011**, *21*, 8887−8892.
(28) De Souza, R. F. B.; Tusi, M. M.; Brandalise, M.; Dias, R. R.; Linardi, M.; Spinace, E. V.; dos Santos, M. C.; Neto, A. O. *Int. J. Electrochem. Sci.* **2010**, *5*, 895−902.
(29) Yuan, Q.; Zhou, Z.; Zhuang, J.; Wang, X. *Chem. Mater.* **2010**, *22*, 2395−2402.
(30) Oliveira, R. T. S.; Santos, M. C.; Nascente, P. A. P.; Bulhoes, L. O. S.; Pereira, E. C. *Int. J. Electrochem. Sci.* **2008**, *3*, 970−979.
(31) Kowal, A.; Li, M.; Shao, M.; Sasaki, K.; Vukmirovic, M. B.; Zhang, J.; Marinkovic, N. S.; Liu, P.; Frenkel, A. I.; Adzic, R. R. *Nat. Mater.* **2012**, *8*, 325−330.
(32) Zhang, Y.; Janyasupa, M.; Liu, C. W.; Li, X.; Xu, J.; Liu, C. C. *Adv. Funct. Mater.* **2012**, *22*, 3570−3575.
(33) Choi, J. H.; Park, K. W.; Park, I. S.; Nam, W. H.; Sung, Y. E. *Electrochim. Acta* **2004**, *50*, 787−790.
(34) Park, K. W.; Choi, J. H.; Lee, S. A.; Pak, C.; Chang, H.; Sung, Y. E. *J. Catal.* **2004**, *224*, 236−242.
(35) Park, K. W.; Han, D. S.; Sung, Y. E. *J. Power Sources* **2006**, *163*, 82−86.

(36) Baraldi, A.; Bianchettin, L.; de Gironcoli, S.; Vesselli, E.; Lizzit, S.; Petaccia, L.; Comelli, G.; Rosei, R. *J. Phys. Chem. C* **2011**, *115*, 3378−3384.
(37) Yuge, K.; Ichikawa, T.; Kawai, J. *Mater. Trans., JIM* **2010**, *51*, 321−324.
(38) Liu, L.; Pippel, E.; Scholz, R.; Gosele, U. *Nano Lett.* **2009**, *9*, 4352−4358.
(39) Kakade, B. A.; Tamaki, T.; Ohashi, H.; Yamaguchi, T. *J. Phys. Chem. C* **2012**, *116*, 7464−7470.
(40) Wang, L.; Imura, M.; Yamauchi, Y. *ACS Appl. Mater. Interfaces* **2012**, *4*, 2865−2869.
(41) Guo, S.; Dong, S.; Wang, E. *ACS Nano* **2010**, *4*, 547−555.
(42) Rajeswari, J.; Viswanathan, B.; Varadarajan, T. K. *Mater. Chem. Phys.* **2007**, *106*, 168−174.
(43) Huang, S. Y.; Ganesan, P.; Popov, B. N. *ACS Catal.* **2012**, *2*, 825−831.
(44) Pan, H. B.; Wai, C. M. *New J. Chem.* **2011**, *35*, 1649−1660.
(45) Wang, C.; Daimon, H.; Onodera, T.; Koda, T.; Sun, S. *Angew. Chem., Int. Ed.* **2008**, *47*, 3588−3591.
(46) Kundu, S.; Liang, H. *Langmuir* **2010**, *26*, 6720−6727.
(47) Saidani, F.; Rochefort, D.; Mohamedi, M. *Electrocatal.* **2011**, *2*, 114−122.
(48) Chen, S.; Sheng, W.; Yabuuchi, N.; Ferreira, P. J.; Allard, L. F.; Horn, Y. S. *J. Phys. Chem. C* **2009**, *113*, 1109−1125.
(49) Rao, C. V.; Viswanathan, B. *J. Phys. Chem. C* **2009**, *113*, 18907−18913.
(50) Loukrakpam, R.; Wanjala, B. N.; Yin, J.; Fang, B.; Luo, J.; Shao, M.; Protsailo, L.; Kawamura, T.; Chen, Y.; Petkov, V.; Zhong, C. J. *ACS Catal.* **2011**, *1*, 562−572.
(51) Sasaki, K.; Naohara, H.; Cai, Y.; Choi, Y. M.; Liu, P.; Vukmirovic, M. B.; Wang, J. X.; Adzic, R. R. *Angew. Chem., Int. Ed.* **2010**, *49*, 8602−8607.
(52) Tiwari, J. N.; Tiwari, R. N.; Chang, Y. M.; Lin, K. L. *ChemSusChem* **2010**, *3*, 460−466.
(53) Taylor, E.; Chen, S.; Wu, J. T. L.; Zhu, Y. J. Chen *ChemSusChem* **2010**, *6*, 1863−1867.
(54) Maiyalagan, T. *J. Solid State Electrochem.* **2009**, *13*, 1561−1566.
(55) Guo, J. W.; Zhao, T. S.; Prabhuram, J.; Chen, R.; Wong, C. W. *Electrochim. Acta* **2005**, *51*, 754−763.
(56) Friebel, D.; Miller, D. J.; Nordlund, D.; Ogasawara, H.; Nilsson, A. *Angew. Chem., Int. Ed.* **2011**, *50*, 10190−10192.
(57) Choi, J. H.; Park, K. W.; Kwon, B. K.; Sung, Y. E. *J. Electrochem. Soc.* **2003**, *150*, A973−A978.
(58) Wang, S.; Jiang, S. P.; Wang, X.; Guo, J. *Electrochim. Acta* **2011**, *56*, 1563−1569.
(59) Jiang, J.; Kucernak, A. *J. Electroanal. Chem.* **2003**, *543*, 187−199.
(60) Housmans, T. H. M.; Wonders, Ad H.; Koper, M. T. M. *J. Phys. Chem. B* **2006**, *110*, 10021−10031.
(61) Jusys, Z.; Kaiser, J.; Behm, R. J. *Langmuir* **2003**, *19*, 6759−6769.
(62) Ota, Y.; Nakagawa, M.; Takahashi, M. *J. Electroanal. Chem.* **1984**, *179*, 179−186.
(63) Khazova, O. A.; Mikhailova, A. A.; Skundin, A. M.; Tuseeva, E. K.; Havranek, A.; Wippermann, K. *Fuel Cells* **2002**, *2*, 99−108.
(64) Gojkovic, S.Lj.; Vidakovic, T. R.; Durovic, D. R. *Electrochim. Acta* **2003**, *48*, 3607−3614.
(65) Kluson, P.; Scaife, S. J. *J. Porous Mater.* **2002**, *9*, 115−129.
(66) Young, A. P.; Colbow, V.; Harvey, D.; Rogers, E.; Wessel, S. *J. Electrochem. Soc.* **2013**, *160*, F381−F388.
(67) Gong, X. Q.; Liu, Z. P.; Raval, R.; Hu, P. *J. Am. Chem. Soc.* **2004**, *126*, 8−9.
(68) Saida, T.; Ogiwara, N.; Takasu, Y.; Sugimoto, W. *J. Phys. Chem. C* **2010**, *114*, 13390−13396.
(69) Shao, Y.; Yin, G.; Gao, Y. *J. Power Sources* **2007**, *171*, 558−566.